Independent Component Analysis Filter for Small Vessel Contrast Imaging During Fast Tissue Motion

Wahyulaksana, Geraldi; Wei, Luxi; Schoormans, Jasper; Voorneveld, Jason; Van der Steen, Antonius F.W.; De Jong, Nico; Vos, Hendrik J.

Important note
To cite this publication, please use the final published version (if applicable).
Please check the document version above.

Independent Component Analysis Filter for Small Vessel Contrast Imaging During Fast Tissue Motion

Geraldi Wahyulaksana[1], Luxi Wei[1], Jasper Schoormans[1], Jason Voorneveld[1], Antonius F.W. van der Steen[1], Nico de Jong[1,2], Hendrik J.Vos[1,2]

[1]Biomedical Engineering, Cardiology, Erasmus MC University Medical Center Rotterdam, the Netherlands,
[2]Medical Imaging, ImPhys, Faculty of Applied Sciences, Delft University of Technology, Delft, the Netherlands

Abstract— **Suppressing tissue clutter is an essential step in blood flow estimation and visualization, even when using ultrasound contrast agents. Blind source separation (BSS)-based clutter filter for high frame rate ultrasound imaging has been reported to perform better in tissue clutter suppression than the conventional frequency-based wall filter and nonlinear contrast pulsing schemes. The most notable BSS technique, singular value decomposition (SVD) has shown compelling results in cases of slow tissue motion. However, its performance degrades when the tissue motion is faster than the blood flow speed, conditions which are likely to occur when imaging the small vessels, such as in the myocardium. Independent component analysis (ICA) is another BSS technique that has been implemented as a clutter filter in the spatiotemporal domain. Instead, we propose to implement ICA in the spatial domain where motion should have less impact. In this work, we propose a clutter filter with the combination of SVD and ICA to improve the contrast-to-background ratio (CBR) in cases where tissue velocity is significantly faster than the flow speed. In an *in vitro* study, the range of fast tissue motion velocity was 5-25 mm/s and the range of flow speed was 1-12 mm/s. Our results show that the combination of ICA and SVD yields 7 – 10 dB higher CBR than SVD alone, especially in the tissue high-velocity range. The improvement is crucial for cardiac imaging where relatively fast myocardial motions are expected.**

Index Terms—**Contrast-enhanced ultrasound, clutter filter, slow blood flow, tissue motion, blind source separation**

I. INTRODUCTION

Contrast-enhanced Ultrasound (CEUS) imaging is a diagnostic tool in clinical practice that enables the assessment of microvascular flow and perfusion [1]–[4]. By intravascular injection, encapsulated microbubbles act as ultrasound contrast agents (UCA) that lit up the otherwise hypoechoic blood regions since they produce strong back-scatter signal upon ultrasound insonification. This enhancement improves ultrasound sensitivity to detect vascular flow and allows quantitative evaluation of microvascular flow [5]. Regional microvessel characterization with CEUS, such as characterizing focal liver lesions [2], [6] and renal masses[1] has been recommended and is performed in clinical practice. Moreover, CEUS for detecting myocardial blood flow and perfusion has been used for decades [7], [8], albeit with a limited accuracy to detect regional perfusion deficits [9], [10]. Actually, resolving the flow of contrast agents in the myocardial vascular structure, rather than just detecting the presence of contrast agents, could improve diagnostic assessment [11], [12]. However, quantitative CEUS results have significant variations due to scanner settings, patients physiological variations, and factors relating to the microbubbles [13], [14]. Cardiac imaging has additional problems due to substantial tissue motion. The peak cardiac motion around the location of the left coronary artery has a speed of up to 56mm/s [15]. This rapid motion causes strong tissue clutter artifacts that impair the contrast signal visibility [16].

In the past decades, two main approaches have been developed to suppress the strong tissue clutter that conceals the microbubble flow signal. The first one is frequency-based wall clutter filters for ultrasonic flow imaging, which operate in the temporal domain [17], [18]. It works with the assumption that the flow inside the vessel is faster than the tissue motion, which is not the case with the combination of slow flow in the microvasculature and the fast-moving tissue, causing spectral contents overlap in temporal domain [19]. The second approach is by using contrast specific imaging techniques that exploit the nonlinear properties of microbubbles [20]. One option is by imaging of the harmonic signals of the transmit frequency (subharmonic, second harmonic, superharmonic) [21]–[23]. The alternative is by transmitting a sequence of pulses that cancel the linear tissue components when combined, yet retain nonlinear contrast signal components; such as pulse inversion (PI) [24], amplitude modulation (AM) [25], and power modulated pulse inversion (PMPI / CPS) [26]. However, ultrasound also propagates non-linearly through tissue, which diminishes the contrast between tissue and microbubble non-linear signal, thus reducing contrast visibility [27]. Moreover, since the nonlinear signals have lower signal amplitude and multiple transmit-receive events are combined, noise can become a significant factor [28]. Lastly, contrast-specific pulsing sequences need very well-controlled transmit signals to work optimally in actual clinical settings [29].

More recently, blind source separation (BSS) techniques, which attempt to estimate the original sources of signal mixtures without the information of the mixing process and the

This article has been accepted for publication in a future issue of this journal, but has not been fully edited. Content may change prior to final publication. Citation information: DOI 10.1109/TUFFC.2022.3176742, IEEE Transactions on Ultrasonics, Ferroelectrics, and Frequency Control

2

sources, received a lot of attention as clutter filters [30]. Singular value decomposition (SVD) [31], [32] and independent component analysis (ICA) [33] have shown potential to outperform conventional temporal filters, as they discriminate the clutter and flow signal by their spatiotemporal statistical properties instead of just temporal information. This however means that a BSS clutter filter assumes that the *underlying* statistics in, and between, the image pixels are stationary. This is not necessarily true in medical imaging: In presence of motion, clutter statistics per pixel can change over time since the image moves over the pixels. Hence, the motion within the sample period should be limited, and sufficient frame rate is required, to maintain coherence throughout the filtering interval [34]. Low temporal sampling rates (provided by conventional line-by-line scanning) cause loss of spatiotemporal coherence which makes clutter removal ineffective.

Breakthroughs in ultrafast ultrasonic imaging have enabled the acquisition of more than 1000 images per second, which is an order of magnitude higher than conventional line-by-line scanning. The fast acquisition is achieved by transmitting broad beams that scan the whole field of view with a limited number of beams, instead of line-by-line focused beams [35], [36]. Along with coherent compounding of multiple transmission events (e.g. angled plane-waves), the ultrafast ultrasound approach can produce high temporal sampling images without significant quality degradation compared to line-by-line scanning [37], [38].

SVD is a BSS method based on eigen decomposition that uses second-order statistics (i.e., variance) as the objective function, projecting the data onto orthogonal subspaces and ranking the singular vectors based on their eigenvalues. SVD filtering of high-framerate ultrasound images has been proven to be significantly more effective than conventional temporal filtering for clutter suppression in flow imaging of small vessels [39]. Typically, SVD filters assume that the tissue, flow, and noise components can be decomposed into distinct rank subspaces, ordered (decreasingly) by the magnitude of their eigenvalues. Subsequently, a threshold can be applied to remove the unwanted components, with a low rank threshold for tissue removal and a separate high rank threshold for noise suppression. Several estimators have been investigated and it was reported that the optimal threshold could be estimated using the correlation matrix of the spatial singular vectors [40]. However, SVD performance to suppress clutter drops off significantly with slower flow rate and faster tissue motion [39], [41]. The SVD filter operates on the assumption that the tissue signal has a low spatiotemporal correlation with the microbubble signal. However, their spatiotemporal correlation increases with tissue motion as the tissue encloses the vessels, which causes the decomposition to be less effective. Motion compensation on beamformed images before an SVD filter was investigated but the contrast to background ratio (CBR) improvement was not significant [41]. A combination of non-linear imaging schemes (AM) with SVD was also investigated and were shown to attain worse CBR than only SVD filter [42]. Lastly, clustering the ranks based on the singular values, spatial correlation, and mean Doppler frequency with the K-means algorithm instead of choosing a threshold was proposed to improve the clutter and flow distinction [43]. Although K-means clustering improves the performance, it is still limited by the efficacy of SVD to separate clutter and flow into different components. It could not resolve the case when the tissue motion is significantly faster than the flow speed, which causes the resulting decomposed components to still consist of mixtures of clutter and flow signals.

ICA is another BSS technique that has been investigated as clutter filter [44]. Where SVD transforms data onto a basis with orthogonal vectors; ICA seeks to transform the data onto a basis with statistically independent vectors. In doing so, ICA might provide better results than SVD when the components are correlated in time. With the assumption that the microbubbles are sparser than tissue signal [30], [39], their respective statistical distribution are different and independent of each other, regardless of the tissue motion. Recently, Tierney et al [45] have shown that in combination with ultrafast ultrasound imaging, ICA is better than SVD in detecting slow flow when the tissue velocity is low and displacement is small. However, their ICA implementation over long SVD ensemble and component selection based on power Doppler image rely upon the assumption that large displacement does not occur through the ensemble period. Such assumption is likely to be violated in cardiac imaging, where fast tissue motion and large displacement exist throughout the cardiac cycle.

With the aim of detecting slow flow during high velocity tissue motion, we propose a combination of SVD and ICA as a clutter filter with high-framerate CEUS plane-wave images. Instead of implementing ICA on the spatial singular vectors that represent the flow signals in the entire SVD ensemble duration, we use ICA on a pre-filtered images in a short time window where the flow location is almost static. SVD is used as a pre-filter to remove any semi-static clutter and tissue components. Subsequently the ICA algorithm is employed to further isolate microbubble signal from the residual clutter. Here, it operates as a spatial filter on a subset of images that are almost spatially stationary, enabled by the ultrafast imaging framerate. The signal that consists of microbubble or clutter signal will be unmixed based on their distinct statistical distribution [46]. We chose the fourth-order statistics (normalized kurtosis) as the selection parameter in ICA as it is correlated with ultrasound scatter density [30], [47]. We evaluated and compared the performance of our proposed filter to SVD in an *in vitro* setup where the induced motion simulates realistic cardiac velocity and in a range of slow flow speeds.

II. METHODS

A. *In vitro* Setup

A tissue-mimicking wall-less flow phantom was used for in vitro data acquisition, see Fig. 1. The phantom was made from a suspension of 10% w/v polyvinyl alcohol (PVA) and 1% w/v silicon carbide as background scattering particles, with one completed freeze-thaw thermal cycle. Diluted in-house phospholipid-coated microbubbles (F-type [48], concentration ~ 7.6 x 10^5 MB/mL), which have similar performance to the commercially available Target-Ready MicroMarker (FUJIFILM VisualSonics, Inc.), were used. They were continuously infused through a 1 mm diameter channel by a syringe pump (AL-1000, World Precision Instruments, Sarasota, FL). An ultrasound probe (see below) was attached

to a linear motorized stage. Rigid tissue motion was emulated by moving the probe during image acquisition in various directions. The diagonal direction had 45° angle with both the vertical and horizontal direction, in-plane with the probe image plane; see arrows on left-top in Fig. 1. Initially the tube was located at 2.5 cm depth inside the image; as the probe was moving away from the phantom, the depth was up to 4.3cm.

To test the efficacy of the filter performance, 2 series of experiments were performed: the first investigated the effect of tissue motion while keeping flow speed constant (Table 1) and the second investigated the effect of flow speed while keeping the tissue motion constant (Table 2). These velocities are realistic for cardiac imaging except for peak-early diastolic and peak-early systolic motion [15]. Reported flow speeds in this channel were calculated by the ratio of the flow rate (provided by the perfusion pump setting) and the channel cross-sectional area and hence is the average flow speed, not peak flow speed.

B. Ultrasound Acquisition and Beamforming

RF acquisitions were performed with a linear transducer array (L7-4, Philips ATL, Bothell, WA), connected to a Vantage 256 system (Verasonics Inc., Redmond, WA). Each experiment was repeated 3 times. The transmission sequence consisted of 5 tilted plane waves from -7° to 7° with 3.5° increments with a pulse repetition frequency of 5,000 Hz. The transmitted pulses had a center frequency of 5.2 MHz (4 cycles, fundamental imaging) at a mechanical index (MI) of 0.05, measured with a standard hydrophone setup (30 mm from the transducer). Delay-and-sum beamforming and angular compounding was performed with the Ultrasound Toolbox [50] in Matlab (2020B, the Mathworks, Natick, 2020) on a 0.5 λ resolution grid.
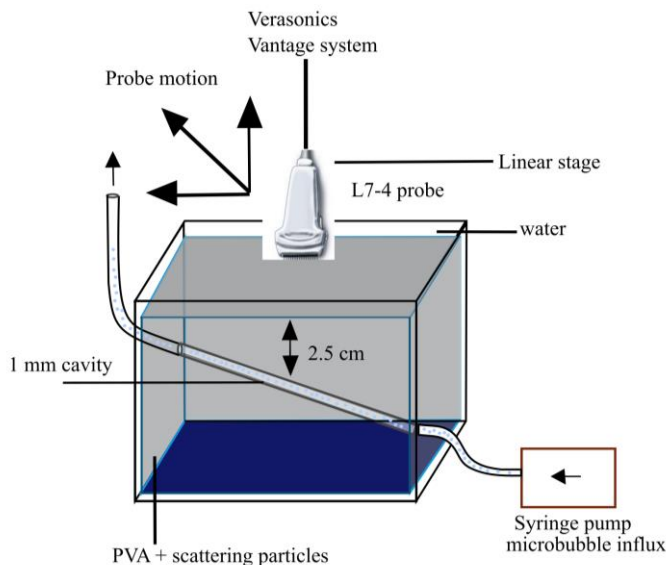

Fig. 1. Experimental setup to investigate the effect of probe motion and flow speed. The flow phantom consists of tissue-mimicking material (gray area) and a 1 mm wall-less cavity to emulate a small vessel. The probe was attached to a linear stage and moved during an acquisition while microbubbles were continuously injected.

TABLE I
PARAMETERS OF PROBE MOTION EXPERIMENT

Probe motion experiment	
Probe axis	Diagonal, axial, lateral
Probe velocity	0, 5, 10, 15, 20, 25 mm/s
Average flow speed	6 mm/s

TABLE II
PARAMETERS OF FLOW SPEED EXPERIMENT

Flow speed experiment	
Probe axis	Diagonal
Probe velocity	25 mm/s
Average flow speed	1, 2, 3, 6, 8, 12 mm/s

C. Two-step BSS framework rationale

A sequence of beamformed contrast-enhanced ultrasound images (s) can be modeled as a linear mixture of 3 independent components: tissue clutter signal (c), microbubble signal (b), and noise (n):

$$s(x,z,t) = c(x,z,t) + b(x,z,t) + n(x,z,t), \qquad (1)$$

where x is lateral position, z is axial position, t is time. To accurately assess the flow signal, the clutter and noise need to be removed from the signal mixture. However, only the observed mixture signal is available, both the mixing process and the source signals are unknown.

Demené et al. [39] have implemented an SVD filter by rearranging the $s(x,z,t)$ as a 2D Casorati matrix S where the dimension is ($n_x \times n_z, n_t$). It was assumed that the tissue clutter has high internal spatiotemporal coherence and is uncorrelated with the flow signal. Therefore, clutter and microbubble signal are expected to be projected into separate singular vectors. The strong tissue clutter would be accumulated in the first few ranks. The microbubble flow signal then can be retrieved by adding the components above an estimated rank threshold.

Although SVD works effectively when the tissue motion is not significantly faster than the flow speed, its performance drops off relatively proportional with tissue motion velocity and inversely proportional with flow velocity [39], [41]. In such case, the assumption of independent motion between tissue and flow is violated as they are temporally correlated. Since SVD maximizes the variance in the spatiotemporal domain, the projected components do not necessarily correspond to isolated signal sources (c, b, n). They could still consist of clutter and microbubble signal mixture, which makes SVD filtering by ranks removal ineffective. As a result, further filtering is needed to resolve flow signal, when it is significantly slower than the tissue motion velocity.

Differently than SVD, ICA finds maximally independent components from linear signal mixtures. The principle lies in the central limit theorem, which states that the linear combination of independent components is closer to a Gaussian distribution than the components prior to the mixing process.
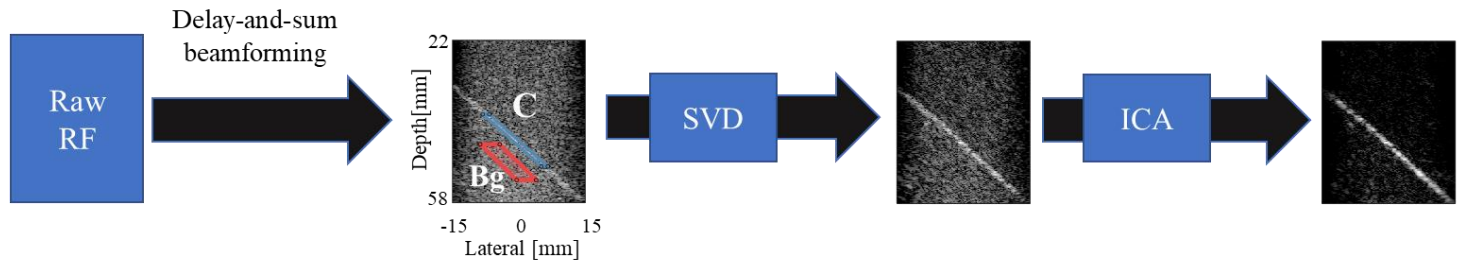
Fig. 2. Overview of the BSS filter framework. Example of regions of interest for calculating CBR. C (blue box) was used for contrast signal strength and Bg (red box) was used for background signal strength. Image is displayed with 40dB dynamic range.

Accordingly, a measure of non-Gaussianity can be used as an objective to obtain maximally independent components; presuming that the sources are independent and have distinct non-Gaussian distribution. The pixel value in ultrasound images $s(x, z, t)$ is a linear summation of tissue, microbubbles and noise that are spatially independent and have different scatterer density, thus distinct spatial distribution. ICA then can be implemented in the spatial domain to retrieve these initial signal components, whereas subsequent images act as independent observations of the spatial distribution. Thus, motion should be less of a factor in spatial domain, compared to the SVD filter that operates in spatiotemporal domain.

Normalized kurtosis (or fourth-order marginal cumulant of a distribution) is adopted as the ICA objective function as it is a measure of non-Gaussianity and has been employed to characterize ultrasound scatterers spatial density/sparsity [30], [47]. However, it is sensitive to other components that have sparse distribution such as strong specular reflections, and noise, in the image, which could be falsely detected as microbubble signal. To improve ICA detection robustness, we therefore propose to first remove the more coherent tissue components, and the incoherent noise, with SVD. This pre-filtered data then will be processed by ICA to further separate the contrast signal from the residual tissue signal. The overview of the processing framework is shown in Fig. 2.

i. SVD as a pre-filter

The input of our ICA implementation is several observations of the signal mixtures that consist of similar spatial structure, i.e., a limited number of subsequently recorded images without coherent plane-wave compounding. High frame rate imaging with tilted plane wave transmissions assure that a similar underlying spatial structure is present in a short ensemble of images, and the SVD filtering [39] is separately performed on subsets of equal transmission angle. The ensemble length for this SVD pre-filtering is found by parametric testing (see Appendix). The noise threshold (nn) is found by the maximum acceleration of the normalized ordered singular values [49]. Additionally, this search starts after 20% of the total singular values number to avoid finding the clutter cutoff. After removing the noise components, the spatial covariance technique is employed to find the clutter cutoff (nc) [50]. Clutter filtering in this first step is described as:

$$\widetilde{S_{bc}}(x, z, t, \alpha) = \sum_{i=nc}^{nn} \lambda_i U_i(x, z, \alpha) V_i(t, \alpha), \quad (2)$$

where $\widetilde{S_{bc}}(x, z, t, \alpha)$ is the filtered images on each transmission angle α, λ are the singular values, U are the spatial singular vectors, and V are the temporal singular vectors. An example of the described rank selection is shown in Fig. 3.
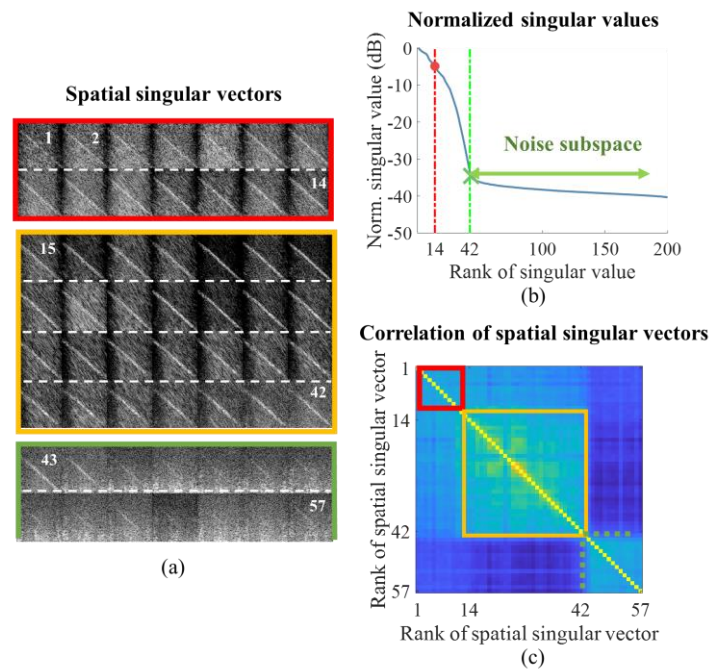

Fig. 3. An example of SVD rank selection. (a) The spatial singular vectors from rank 1 to 57. Components 1 to 14 are deemed as clutter although some minor bubble signal is present, 15 to 42 are mixtures of bubble and clutter, and 43 until 200 are noise. (b) Normalized singular values that were used to determine the noise subspace. (c) Correlation of spatial singular vectors.

ii. ICA filtering

ICA is then implemented on the output of the SVD filter in the first step to further separate microbubble signal and clutter. The algorithm was applied to an observation window (y) of an ensemble length (el), which arranged as a Casorati matrix with dimension ($n_x \times n_z$, $n_\alpha \times n_{el}$). The angled images (without coherent compounding) were used as input to provide different observations of the imaged object and to preserve framerate. Sequential observation windows were constructed from $\widetilde{S_{bc}}$. The ensemble length should be short to keep the stationarity of the superimposed signal but long enough to provide several observations of the mixture; we tested a range of ensemble lengths to find the reasonable trade-off, as reported in the Appendix. Both real and imaginary part of the signal were used.

Pre-whitening, which normalized the observed data to achieve faster convergence, is not performed because removing the eigenvalue of the components highlighted the clutter or noise components that were not removed by SVD. The robust ICA algorithm was chosen because it can process complex-valued signals and does not require pre-whitening to achieve fast convergence [51]. It is applied on each window to maximize the non-Gaussianity of the estimated sources:

$$y = WS, \tag{3}$$

where W is the temporal mixing matrix and S is the maximally independent spatial components. Since no pre-whitening is applied, the resulting independent components are direct linear combination of the observation window. The components are then sorted by their normalized kurtosis value (S_{sort}). Since microbubble signals are sparser and thus have higher kurtosis than tissue, the approximated microbubble signal ($\widetilde{s}_b$) is retrieved from the mixture by adding the components (nk) that have kurtosis higher than a defined threshold:

$$\widetilde{s}_b(x, z) = \sum_{i=1}^{nk} S_{sort}(x, z, i). \tag{4}$$

The kurtosis threshold needs to be adjusted based on the distribution of the microbubbles that are present in the images. Empirically, we found kurtosis threshold of 45 worked well for our dataset and we used this value for all subsequent analysis. Since the noise has been reduced in the pre-filter step, only one threshold is needed. An example of the described rank selection is shown in Fig. 4.
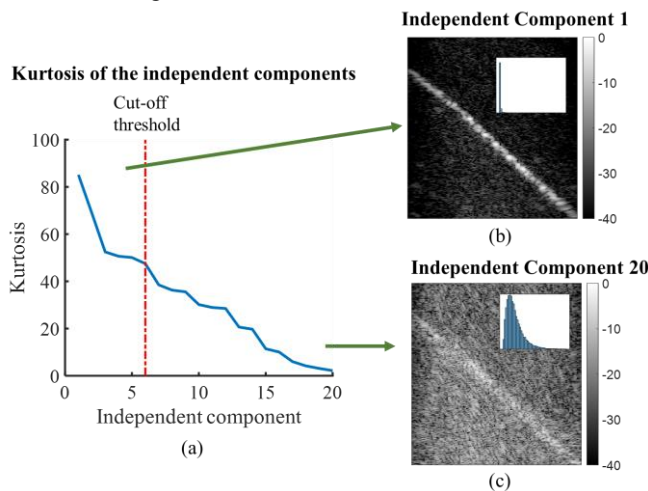

Fig. 4. An example of ICA ranking. (a) The kurtosis of all the calculated independent components. (b+c) B-mode images of some selected components in logarithmic scale and their respective normalized histogram of the pixel magnitude as inset. (b) The independent component with highest kurtosis. (c) The independent component with lowest kurtosis.

D. Post processing

To perform quantitative analysis, regions of interest (ROIs) were manually drawn (Fig. 2.) on the tube (contrast) and PVA (background), which then automatically followed (by a global motion estimator via 2D cross correlation) the tube and PVA while the probe was moving. Contrast-to-background ratio

(CBR) was then calculated to evaluate the filters' performances to suppress clutter signal, defined as:

$$CBR = 20 \log_{10} \left(\frac{\overline{RMS}_{contrast}}{\overline{RMS}_{background}} \right), \tag{5}$$

where $\overline{RMS}$ is the time-averaged root-mean-square signal strength in a time interval (0.4 seconds) during which the probe velocity was constant.

III. RESULTS

A. Implementation of SVD and ICA filters

Several SVD ensemble lengths were tested for different probe speeds but no significant differences were observed for the results with different ensemble lengths; see Appendix Fig. A. We chose an ensemble length of 200 frames for all subsequent analyses. Several ensemble lengths for the ICA implementation were also examined (see Appendix Fig. B). An ensemble length of 20 frames, which provided the optimal CBR, was chosen.
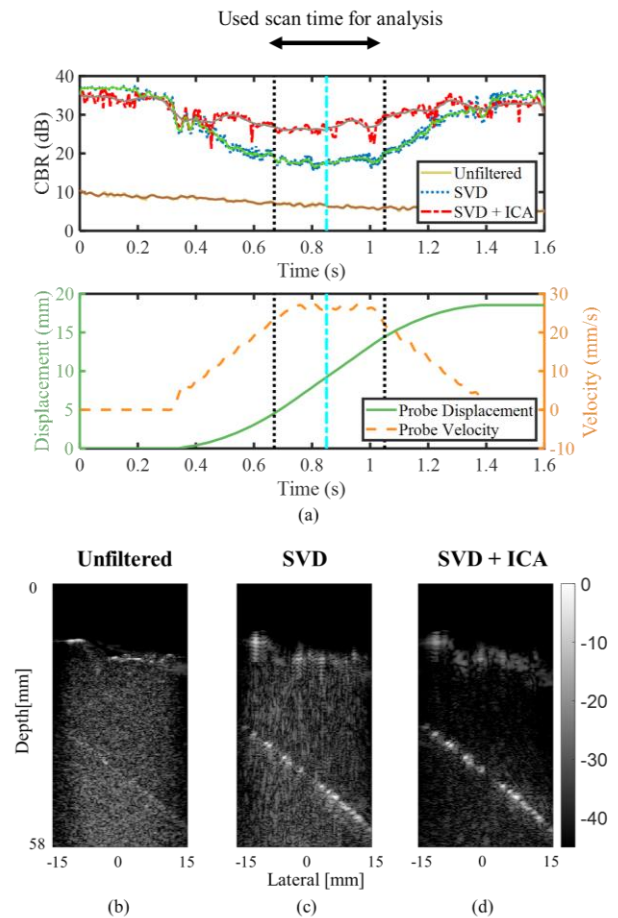
Fig. 5. Effect of probe motion (a) CBR during 25mm/s probe axial motion experiment and sample images during constant nominal velocity (t=0.85s, cyan line) after processing, (b) Unfiltered beamformed image, (c) SVD, and (d) SVD + ICA.

An example of an acquisition analysis and the result of the filter implementations are shown in Fig. 5. The CBR in the filtered images correlated with the probe velocity, while the CBR in the unfiltered images was not influenced by the probe

motion, as expected. During the time interval when the probe was not moving, both SVD and SVD + ICA filter achieved similar CBR (~33 dB). However, SVD + ICA outperformed SVD alone during probe motion. When the probe speed exceeds 10 mm/s (t = 0.5:1.15 s), the CBR of SVD + ICA improves up to 10.5 dB and 20.4 dB compared to SVD alone and the unfiltered signal, respectively. SVD performance declined proportionally with the probe velocity (24.5 dB difference between static and peak probe velocity), while SVD + ICA retained more stable performance during motion on average. Note, this experiment had a contrast flow speed of 6 mm/s, and thus the flow speed is significantly lower than the peak probe speed. As visible in Fig. 5, the curves showed a frame-to-frame variation. Twenty-frames moving average trend lines were calculated. The standard deviation compared to the trend line of the CBR of SVD + ICA line was 1.2 dB, SVD was 0.8 dB, and the non-filtered showed low frame-to-frame variations (0.15 dB).

B. Effect of probe motion

The filters' performance during various probe motion is shown in Fig. 6. In the static situation, simple SVD filter achieved 3 dB higher CBR. However, SVD + ICA consistently outperformed simple SVD during motion experiments, especially in the high velocity ranges (15-25 mm/s). The mean differences between the two filters in the high velocity ranges were 6.7 dB (axial), 6.9 dB (lateral), and 9.9 dB (diagonal). CBR for SVD declined proportionally with the probe speed across the motion direction (~3 dB per 5 mm/s probe speed increment), except for diagonal motion of 20 to 25 mm/s. This downward trend results in a significant CBR difference (9.1 dB in average) between the slowest and the fastest probe speed after SVD filtering. On the other hand, the CBR obtained by SVD + ICA at 25 mm/s probe speed was only marginally lower (3.2 dB on average) than the 5 mm/s probe speed.
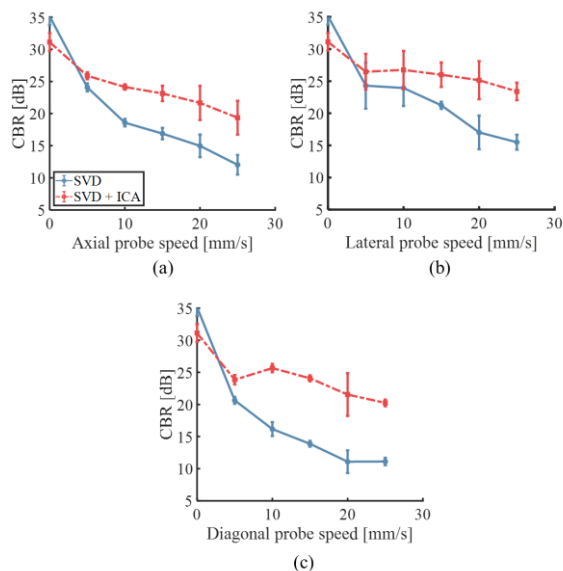

Fig. 6. Contrast-to-background values after processing by SVD and SVD + ICA for a range of probe velocities. The error bars represent the standard deviation from 3 repetitions (a) Axial probe motion, (b) Lateral probe motion, (c) Diagonal probe motion.

C. Effect of Flow Speed

The filters' performance with varying flow speed while the probe was moving in high velocity (25 mm/s) is shown Fig. 7. The result of one acquisition (flow speed 2 mm/s) was removed from subsequent analysis because the microbubble concentration was significantly lower than in other acquisitions, which complicated the contrast-level calculations. Both filters' performances were greatly influenced by the flow speed, where decreasing flow speed was proportional to CBR decline in both SVD and SVD + ICA. Although the SVD + ICA combination still exceeded SVD in all flow speed (6.8 dB on average), the CBR gain reduces with increasing flow speed approaching the probe speed. The CBR for both filters increased by ~4 dB from flow speed 6 mm/s to 8 mm/s; while the CBR only increased by 2.7 dB and 1.3 dB for SVD and SVD + ICA, respectively, from flow speed 8 mm/s to 12 mm/s. The unfiltered data showed a mild increase of few dB of CBR with flow speed.
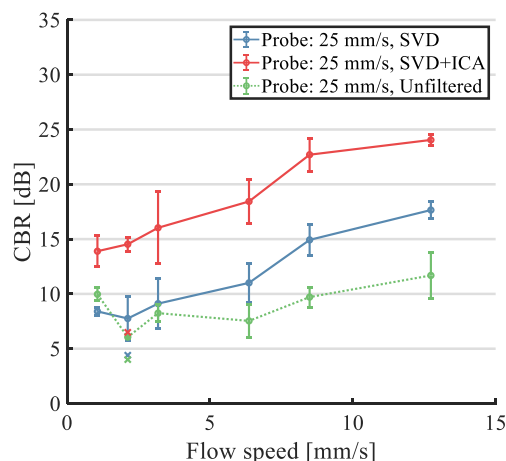

Fig. 7. Contrast-to-background values after processing by SVD and SVD + ICA for a range of flow speeds, while the probe was moving (25 mm/s) diagonally. The contrast-to-background values while the probe was static is provided as baseline reference.

IV. DISCUSSION

In this study, we have shown that SVD+ICA improved the clutter suppression over SVD alone in case of slow flow during realistic velocities of cardiac motion, in an in vitro phantom experiment. Our proposed filter framework consistently achieved better contrast-to-background ratio than SVD during motion, especially in the fastest probe motion (25 mm/s) where ICA exceeded the CBR of the SVD filtered and unfiltered data by approximately 10 dB and 20 dB, respectively. In the static situation, ICA and SVD perform comparably, with slightly higher CBR with SVD alone than ICA. However, in the static condition where CBR is around 30dB, this difference does not have any impact on the contrast visibility. The CBR improvement during motion is presumably due to ICA resolving the output of SVD that still consists of clutter and microbubbles signal mixture. ICA utilizes the different spatial distribution statistics of clutter and microbubbles instead of spatiotemporal coherence like SVD.

We performed an in vitro experiment where the probe motion velocities and directions were modified while keeping the flow

rate fixed. The results show that SVD performance to suppress background clutter signal degrades proportionally with probe speed, while the SVD+ICA retains relatively stable clutter suppression for increasing probe speeds. The trends are consistent across all the motion directions conducted in our experiments (axial, lateral, and diagonal). The ineffectiveness of the SVD filter during motion is consistent with reports by Demené et al. [39] and Zhu et al. [41]. However, to our knowledge, systematic evaluation in the high tissue velocity ranges (up to 25 mm/s) has not been reported before. As opposed to SVD, ICA filtering is affected less by motion because it operates in a short time where motion is negligible, facilitated by high-framerate imaging. This stability of signal might be beneficial for cardiac vascular flow imaging where motion should not influence the readout of the contrast signal.

The effect of different flow rates was assessed while the probe motion was kept constant at the highest velocity (25 mm/s). Clutter suppression of the SVD filter diminished proportionally with lower flow speed, as the spatiotemporal correlation between microbubbles and tissue signals increases. Combination with ICA again improves the CBR over SVD alone by 5-8 dB across all flow speeds. However, this time ICA could not retain stable CBR through different flow rates because the differences between the probe and flow speed are more significant compared to the probe motion experiment. Another possible reason is microbubble disruption. A slower flow rate inherently provides slower microbubbles replenishment, which leads to more acoustically-induced deflation [52], resulting in lower CBR. The lower CBR with lower flow speed is visible in the unfiltered data in Fig. 7. By comparing the unfiltered and SVD-filtered results, it appears that the SVD filtering does not improve CBR at all upon high tissue motion and slow flow, whereas SVD+ICA does lead to higher CBR.

Unlike conventional wall frequency-based wall filters that have real physical representation and thus a meaningful threshold selection, selecting a threshold for BSS methods is not straightforward. Although SVD component selection is a well-known problem, there is still no standardized way to perform it. Initially, Demené et al. [39] used a qualitative approach to obtain optimal SVD threshold selection. Several efforts to solve this issue were published [40], [50], [53], [54], but we did not find any method that worked robustly for our dataset. We found that denoising the matrix by singular values acceleration [54] and using spatial correlation to find the clutter cut-offs [40], [50] worked well for our dataset. Additionally, we manually re-checked all selected automated thresholds and adapted thresholds where necessary. Since the aim of this research was to investigate ICA filter performance, rather than finding a robust method to select the SVD components of the pre-filtering step, we manually adjusted the slow flow acquisitions. As such, we were able to fairly compare filters at their maximum attainable CBR.

Component selection is a major issue for ICA filtering as well. In this study, we sorted the independent components by normalized kurtosis, with the assumption that the microbubble image intensity distribution is sparser than clutter signal. A threshold value that performed well for the dataset was empirically chosen and used for all analyses. The empirical approach means that the selected threshold was tuned

specifically for the microbubble population in the channel of our phantom. As the kurtosis threshold defines the filtering outcome, adjusting the threshold is required for implementation on different imaging targets. This in practice might be solved by using imaging target pre-sets which already is customary in current clinical systems. Additionally, ensemble length also is a parameter that needs to be tuned since our ICA implementation presumes negligible displacement in an observation window. The optimal ensemble length would depend on the acquisition framerate and the motion velocity. It is a trade-off between providing spatial sample and retaining stationarity of underlying statistical structure, which hinges on the velocity of the tissue motion. The ensemble length we used for the analysis was chosen based on empirical evaluation.

Although an *in vitro* setup is more controllable compared to an *in vivo* environment, there are still some experimental uncertainties that influence the quantitative results. Microbubble concentration variabilities is always a factor in quantitative CEUS imaging as it is directly related to the backscattering magnitude, and hence to the CBR 'offset'. The size distribution, stability, and acoustic properties of the microbubbles might be altered because they were diluted and stored in a suspending fluid prior to infusion [55]. Distinct microbubble disruption-replenishment in the varying flow experiment also contributed to the observed CBR variability, especially in the low flow settings. We excluded 1 acquisition (repetition number 3 of flow 2mm/s) because of too low microbubble concentration. Yet, the CBRs of the filters were always obtained from the same initial dataset, thus they are mutually comparable. Lastly, assessment of CBR by calculating the mean of the pixel values in the ROIs might introduce some bias towards the contrast detection sensitivity because the tube is not always completely filled with microbubbles. Region-of-interest locations that were drawn manually might have introduced some uncertainties to the CBR calculation. However, the comparison between different filters and unfiltered signal are not affected by this bias as the same ROIs in a single acquisition were used for all methods.

It should be noted that the performance of ICA depends on SVD to remove the semi-static clutter and noise. In our implementation, ICA needs the contrast signal to be stronger than the tissue signal (positive CBR) to operate. Since the pre-filtering is an important step and SVD still has some concerns by itself (component selection and performance in motion); it is worth to consider other methods as a substitute for the pre-filter step in the future. A possible solution could be contrast-specific detection scheme like AM, PI, or PMPI that suppress tissue signal while retaining larger part of the contrast signal. The utilization of motion compensation before implementing the BSS filter is one of the possible improvements of the technique. However, to date, there is no standardized motion compensation algorithm that can be implemented straightforwardly. Several studies implemented various motion compensation algorithm and reported disparate improvements [41], [56], [57]. Since ICA will also benefit from a proper implementation of motion compensation, ICA should also be tested on the motion corrected images when making the comparison with only SVD filtering. Another direction of improvement would be a more robust ICA component selection. Instead of defining a fixed kurtosis threshold, fitting

the components to a specific distribution like the homodyned K-distribution that gives a physical meaning [58] or the Nakagami distribution that is proven to describe *in vivo* data [59] might provide more stability compared to thresholding by normalized-kurtosis. Alternatively, algorithmically defined threshold like suggested by Tierney et al [45] yet adapted for high velocity case could be an option. The 2-step processing induces extra computational cost. Although the computational time to perform SVD will be multiplied by the number of the transmission angles, the increase is not substantial since the time needed to process an ensemble of 200 frames is relatively short (~2 seconds). On the other hand, ICA requires more substantial time (15-20 minutes) in the current non-optimized implementation. However, we are trying to resolve the contrast detection and not aiming for real time or fast processing for now. In the future, more efficient operation could be implemented to reduce the computation time.

Translation to clinical application needs a further validation since our *in-vitro* setup simplifies the *in-vivo* conditions in several aspects. First, the myocardium tissue scatterers are inhomogeneous, which might impair the bubble detection mechanism. However, the assumptions that microbubble and tissue (myocardium) have different spatial scatterers' distribution should still be applicable. The fast-flowing microbubbles in the cardiac chamber, that are not relevant for perfusion imaging, can be removed by using a low pass filter to enhance the sparsity of the microbubble signals in the myocardium. Second, the size of the vessel determines the number of bubbles that are present, which affects the magnitude of the flow signal. The cavity diameter in our flow phantom (1 mm) is in the range of the small coronary arteries sizes. On the other hand, likely the microcapillaries (~10 µm) could not be detected by ICA because they are small and densely populated (more than 2000 microvessels per mm2 [7]). The fully-developed speckle contrast signal from the microcapillaries will have low kurtosis and will be rejected by the filter. However, we are aiming at visualizing the small vessels and not at resolving the sub-resolution capillary perfusion. Third, cardiac (phased array) probe image resolution is worse and have a substantial depth-dependent resolution, compared to the linear probe that was used in this study. A possible mitigation could be implementing the beamforming and the filtering algorithm in the polar domain in which the resolution will be relatively uniform with depth. Fourth, if severe aberration changes the pixel location of the bubble in the images with different transmission angle, the assumption of our ICA implementation that the microbubbles signal location does not change within the underlying subset of images is violated and the aberration would lead to image deterioration. Fifth, the current measurements only emulate rigid motion and visualize single channel. The non-rigid myocardial motion should not bring a new problem to our ICA implementation that operates in spatial domain; as long as the framerate is high enough to assume stationarity of the underlying statistical structure. Multiple vessels inside the field of view also should not be an issue, provided they are still sparse (see Appendix Fig. C). Lastly, changing the ICA ensemble size did not show a big impact in our in-vitro data (Appendix Fig. B.), yet it might be necessary to re-investigate the optimal length ensemble for in-vivo

application or eventually have that length being automatically tuned to the observed motion in the data.

V. CONCLUSION

We showed that ICA in combination with an SVD pre-filtering step provides better contrast detection, with CBR improvement of 7-10 dB, compared to SVD alone. It is more motion-independent clutter suppression throughout various tissue motion (5 to 25 mm/s) and a range of flow perfusion velocity (1 to 12 mm/s). The improvement and stability of ICA filtering is an essential step for cardiac perfusion imaging, where high myocardial velocities are expected and stable contrast detection facilitates the interpretation.

APPENDIX

Ensemble length is an influential parameter for both SVD and ICA filter implementation. For this reason, we performed a quantitative evaluation (via CBR) to find the optimal ensemble length for both filters, which would be used for the results' analysis. One repetition (400 frames) of the axial probe motion dataset was processed with a range of ensemble lengths and the resulting CBR was compared. The results of the axial probe experiment, processed with the SVD filter (50-400 frames) are shown in Fig. A. There was no optimal ensemble length that could drastically improve the resulting CBR when the probe was moving in different speeds. The shorter ensembles (50 and 100 frames) had higher standard deviations than the longer ensembles (200 and 400 frames). Ensemble lengths of 200 frames seemed to obtain optimal results and hence was chosen for the analysis. Subsequently, the same dataset was processed with SVD filter of 200 frames ensemble and ICA filter (10-25 frames). The results are shown in Fig. B. Ensemble length of 10 frames consistently performed worst, compared to the rest. Ensemble length of 20 frames was chosen as it provided good tradeoff between CBR and framerate. The ensemble lengths for SVD filter (200 frames) and ICA filter (20 frames) were used for all the Figs. in the results section. We performed an additional free hand scanning on a phantom with multiple channels inside the field of view (Fig. C.). The flow in the channels was on the order of 8, 3, and 5 mm/s, set by two independent syringe pumps and asymmetric flow splitting. ICA improves the SVD and unfiltered image data by 1.7 dB and 5 dB, respectively.

This article has been accepted for publication in a future issue of this journal, but has not been fully edited. Content may change prior to final publication. Citation information: DOI 10.1109/TUFFC.2022.3176742, IEEE Transactions on Ultrasonics, Ferroelectrics, and Frequency Control
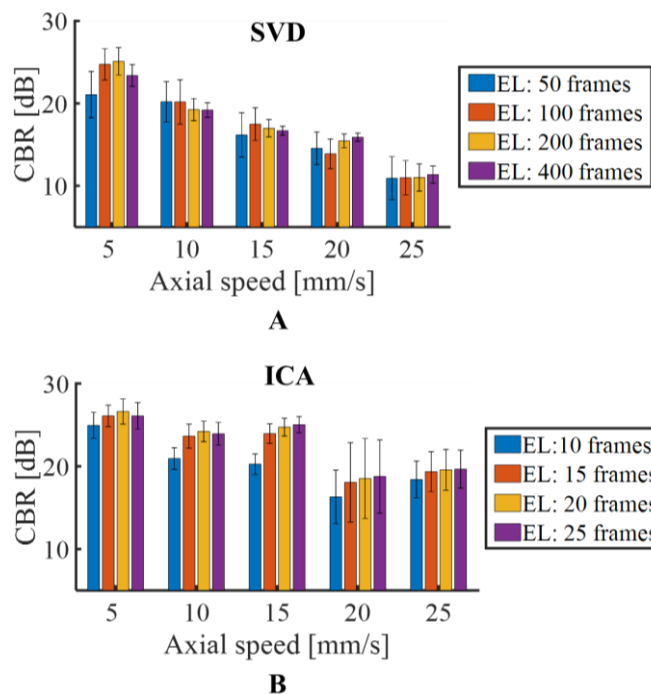
9

Fig. A. SVD and B. ICA implementation for different ensemble lengths in varying probe speed.
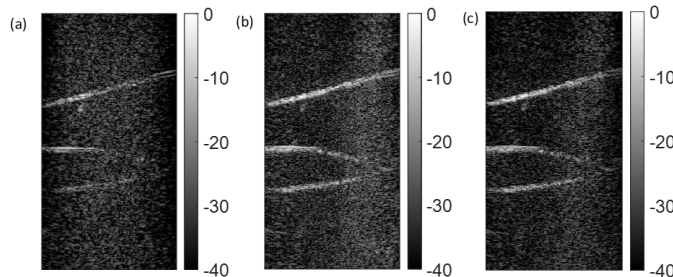

Fig. C. Phantom images during free hand scanning after different processing, (a)Unfiltered beamformed image, (b) SVD, and (c) SVD + ICA.

REFERENCES

[1]   A. S. Paul Sidhu *et al.*, "The EFSUMB Guidelines and Recommendations for the Clinical Practice of Contrast-Enhanced Ultrasound (CEUS) in Non-Hepatic Applications: Update 2017 (Long Version) Die EFSUMB-Leitlinien und Empfehlungen für den klinischen Einsatz des kontrastverstärkten Ultraschalls (CEUS) bei nicht-hepatischen Anwendungen: Update 2017 (Langversion)," *EFSUMB Guidel. Ultraschall Med*, vol. 39, pp. 2–44, 2018, doi: 10.1055/a-0586-1107.

[2]   C. F. Dietrich *et al.*, "Guidelines and Good Clinical Practice Recommendations for Contrast-Enhanced Ultrasound (CEUS) in the Liver–Update 2020 WFUMB in Cooperation with EFSUMB, AFSUMB, AIUM, and FLAUS: WFUMB in Cooperation with EFSUMB, AFSUMB, AIUM and FLAUS," *Ultrasound in Medicine and Biology*, vol. 46, no. 10. Elsevier Inc., pp. 2579–2604, Oct. 01, 2020, doi: 10.1016/j.ultrasmedbio.2020.04.030.

[3]   E. Fröhlich, R. Muller, X.-W. Cui, D. Schreiber-Dietrich, and C. F. Dietrich, "Dynamic Contrast-Enhanced Ultrasound for Quantification of Tissue Perfusion," *J. Ultrasound Med.*, vol. 34, no. 2, pp. 179–196, Feb. 2015, doi: 10.7863/ultra.34.2.179.

[4]   E. Quaia, "Assessment of tissue perfusion by contrast-enhanced ultrasound," *Eur. Radiol.*, vol. 21, no. 3, pp. 604–615, Mar. 2011, doi: 10.1007/s00330-010-1965-6.

[5]   C. Greis, "Quantitative evaluation of microvascular blood flow by contrast-enhanced ultrasound (CEUS)," in *Clinical Hemorheology and Microcirculation*, 2011, vol. 49, no. 1–4, pp. 137–149, doi: 10.3233/CH-2011-1464.

[6]   S. R. Wilson, P. N. Burns, and Y. Kono, "Contrast-Enhanced Ultrasound of Focal Liver Masses: A Success Story," *Ultrasound in Medicine and Biology*, vol. 46, no. 5. Elsevier USA, pp. 1059–1070, May 01, 2020, doi: 10.1016/j.ultrasmedbio.2019.12.021.

[7]   S. Kaul, "Myocardial contrast echocardiography a 25-year retrospective," *Circulation*, vol. 118, no. 3. Lippincott Williams & Wilkins, pp. 291–308, Jul. 15, 2008, doi: 10.1161/CIRCULATIONAHA.107.747303.

[8]   T. R. Porter and F. Xie, "Myocardial Perfusion Imaging With Contrast Ultrasound," *JACC: Cardiovascular Imaging*, vol. 3, no. 2. JACC: Cardiovascular Imaging, pp. 176–187, Feb. 01, 2010, doi: 10.1016/j.jcmg.2009.09.024.

[9]   K. Wei, A. R. Jayaweera, S. Firoozan, A. Linka, D. M. Skyba, and S. Kaul, "Quantification of myocardial blood flow with ultrasound-induced destruction of microbubbles administered as a constant venous infusion," *Circulation*, vol. 97, no. 5, pp. 473–483, Feb. 1998, doi: 10.1161/01.CIR.97.5.473.

[10]   R. Vogel *et al.*, "The quantification of absolute myocardial perfusion in humans by contrast echocardiography: Algorithm and validation," *J. Am. Coll. Cardiol.*, vol. 45, no. 5, pp. 754–762, Mar. 2005, doi: 10.1016/j.jacc.2004.11.044.

[11]   B. F. Osmanski, M. Pernot, G. Montaldo, A. Bel, E. Messas, and M. Tanter, "Ultrafast doppler imaging of blood flow dynamics in the myocardium," *IEEE Trans. Med. Imaging*, vol. 31, no. 8, pp. 1661–1668, 2012, doi: 10.1109/TMI.2012.2203316.

[12]   A. Bauer, L. Solbiati, and N. Weissman, "Ultrasound imaging with SonoVue: Low mechanical index real-time imaging," in *Academic Radiology*, Feb. 2002, vol. 9, no. SUPPL. 2, pp. S282–S284, doi: 10.1016/S1076-6332(03)80204-0.

[13]   M.-X. Tang *et al.*, "Quantitative contrast-enhanced ultrasound imaging: a review of sources of variability," *Interface Focus*, vol. 1, no. 4, pp. 520–539, Aug. 2011, doi: 10.1098/rsfs.2011.0026.

[14]   A. L. Emanuel, R. I. Meijer, E. Poelgeest, P. Spoor, E. H. Serné, and E. C. Eringa, "Contrast-enhanced ultrasound for quantification of tissue perfusion in humans," *Microcirculation*, vol. 27, no. 1, p. e12588, Jan. 2020, doi: 10.1111/micc.12588.

[15]   G. Shechter, J. R. Resar, and E. R. McVeigh,

This article has been accepted for publication in a future issue of this journal, but has not been fully edited. Content may change prior to final publication. Citation information: DOI 10.1109/TUFFC.2022.3176742, IEEE Transactions on Ultrasonics, Ferroelectrics, and Frequency Control

10

"Displacement and velocity of the coronary arteries: Cardiac and respiratory motion," *IEEE Trans. Med. Imaging*, vol. 25, no. 3, pp. 369–375, Mar. 2006, doi: 10.1109/TMI.2005.862752.

[16]   M. Toulemonde *et al.*, "Effects of motion on high frame rate contrast enhanced echocardiography and its correction," Oct. 2017, doi: 10.1109/ULTSYM.2017.8092362.

[17]   L. Thomas and A. Hall, "Improved wall filter for flow imaging of low velocity flow," *Proc. IEEE Ultrason. Symp.*, vol. 3, pp. 1701–1704, 1994.

[18]   S. Bjærum, H. Torp, and K. Kristoffersen, "Clutter filter design for ultrasound color flow imaging," *IEEE Trans. Ultrason. Ferroelectr. Freq. Control*, vol. 49, no. 2, pp. 204–216, 2002, doi: 10.1109/58.985705.

[19]   A. Heimdal and H. Torp, "Ultrasound Doppler Measurements of Low Velocity Blood Flow: Limitations Due to Clutter Signals from Vibrating Muscles," *IEEE Trans. Ultrason. Ferroelectr. Freq. Control*, vol. 44, no. 4, p. 873, 1997.

[20]   M. A. Averkiou, M. F. Bruce, J. E. Powers, P. S. Sheeran, and P. N. Burns, "Imaging Methods for Ultrasound Contrast Agents," *Ultrasound in Medicine and Biology*, vol. 46, no. 3. Elsevier USA, pp. 498–517, Mar. 01, 2020, doi: 10.1016/j.ultrasmedbio.2019.11.004.

[21]   P. N. BURNS, "Harmonic imaging with ultrasound contrast agents," *Clin. Radiol.*, vol. 51, 1996.

[22]   F. Forsberg, W. T. Shi, and B. B. Goldberg, "Subharmonic imaging of contrast agents," *Ultrasonics*, vol. 38, no. 1, pp. 93–98, Mar. 2000, doi: 10.1016/S0041-624X(99)00148-1.

[23]   A. Bouakaz, S. Frigstad, F. J. Ten Cate, and N. de Jong, "Super harmonic imaging: A new imaging technique for improved contrast detection," *Ultrasound Med. Biol.*, vol. 28, no. 1, pp. 59–68, Jan. 2002, doi: 10.1016/S0301-5629(01)00460-4.

[24]   D. Hope Simpson, C. Ting Chin, P. N. Burns, D. H. Simpson, C. T. Chin, and P. N. Burns, "Pulse Inversion Doppler : A New Method for Detecting Nonlinear Echoes from Microbubble Contrast Agents," *372 ieee Trans. Ultrason. Ferroelectr. Freq. Control*, vol. 46, no. 2, pp. 372–382, 1999.

[25]   G. A. Brock-Fisher, "Means for increasing sensitivity in non-linear ultrasound imaging systems," *J. Acoust. Soc. Am.*, vol. 101, no. 6, p. 3240, Jun. 1997, doi: 10.1121/1.418339.

[26]   R. J. Eckersley, C. T. Chin, and P. N. Burns, "Optimising phase and amplitude modulation schemes for imaging microbubble contrast agents at low acoustic power," *Ultrasound Med. Biol.*, vol. 31, no. 2, pp. 213–219, 2005, doi: 10.1016/j.ultrasmedbio.2004.10.004.

[27]   M.-X. Tang, N. Kamiyama, and R. J. Eckersley, "Effects of Nonlinear Propagation in Ultrasound Contrast Agent Imaging," *Ultrasound Med. Biol.*, vol. 36, no. 3, pp. 459–466, Mar. 2010, doi: 10.1016/J.ULTRASMEDBIO.2009.11.011.

[28]   J. Viti, H. J. Vos, N. De Jong, F. Guidi, and P. Tortoli, "Detection of Contrast Agents: Plane Wave Versus Focused Transmission," *IEEE Trans. Ultrason. Ferroelectr. Freq. Control*, vol. 63, no. 2, pp. 203–211, 2016, doi: 10.1109/TUFFC.2015.2504546.

[29]   E. Boni, A. C. H. Yu, S. Freear, J. A. Jensen, and P. Tortoli, "Ultrasound open platforms for next-generation imaging technique development," *IEEE Trans. Ultrason. Ferroelectr. Freq. Control*, vol. 65, no. 7, pp. 1078–1092, Jul. 2018, doi: 10.1109/TUFFC.2018.2844560.

[30]   R. R. Wildeboer *et al.*, "Blind Source Separation for Clutter and Noise Suppression in Ultrasound Imaging : Review for Different Applications," no. C, pp. 1–17.

[31]   L. A. F. Ledoux, P. J. Brands, and A. P. G. Hoeks, "Reduction of the Clutter Component in Doppler Ultrasound Signals Based on Singular Value Decomposition: A Simulation Study," *Ultrason. Imaging*, vol. 19, no. 1, pp. 1–18, Jan. 1997, doi: 10.1177/016173469701900101.

[32]   S. Bjærum, H. Torp, and K. Kristoffersen, "Clutter filters adapted to tissue motion in ultrasound color flow imaging," *IEEE Trans. Ultrason. Ferroelectr. Freq. Control*, vol. 49, no. 6, pp. 693–704, 2002, doi: 10.1109/TUFFC.2002.1009328.

[33]   C. M. Gallippi, K. R. Nightingale, and G. E. Trahey, "BSS-based filtering of physiological and ARFI-induced tissue and blood motion," *Ultrasound Med. Biol.*, vol. 29, no. 11, pp. 1583–1592, 2003, doi: 10.1016/j.ultrasmedbio.2003.07.002.

[34]   A. Yu and L. Lovstakken, "Eigen-based clutter filter design for ultrasound color flow imaging: a review," *IEEE Trans. Ultrason. Ferroelectr. Freq. Control*, vol. 57, no. 5, pp. 1096–1111, May 2010, doi: 10.1109/TUFFC.2010.1521.

[35]   J. Bercoff *et al.*, "Ultrafast compound doppler imaging: Providing full blood flow characterization," *IEEE Trans. Ultrason. Ferroelectr. Freq. Control*, vol. 58, no. 1, pp. 134–147, Jan. 2011, doi: 10.1109/TUFFC.2011.1780.

[36]   M. Tanter and M. Fink, "Ultrafast imaging in biomedical ultrasound," *IEEE Trans. Ultrason. Ferroelectr. Freq. Control*, vol. 61, no. 1, pp. 102–119, 2014, doi: 10.1109/TUFFC.2014.2882.

[37]   G. Montaldo, M. Tanter, J. Bercoff, N. Benech, and M. Fink, "Coherent plane-wave compounding for very high frame rate ultrasonography and transient elastography," *IEEE Trans. Ultrason. Ferroelectr. Freq. Control*, vol. 56, no. 3, pp. 489–506, 2009, doi: 10.1109/TUFFC.2009.1067.

[38]   B. Denarie *et al.*, "Coherent plane wave compounding for very high frame rate ultrasonography of rapidly moving targets," *IEEE Trans. Med. Imaging*, vol. 32, no. 7, pp. 1265–1276, 2013, doi: 10.1109/TMI.2013.2255310.

[39]   C. Demené *et al.*, "Spatiotemporal Clutter Filtering of Ultrafast Ultrasound Data Highly Increases Doppler and fUltrasound Sensitivity," *IEEE Trans. Med. Imaging*, vol. 34, no. 11, pp. 2271–2285, 2015, doi: 10.1109/TMI.2015.2428634.

[40]   J. Baranger, B. Arnal, F. Perren, O. Baud, M. Tanter, and C. Demene, "Adaptive Spatiotemporal SVD

This article has been accepted for publication in a future issue of this journal, but has not been fully edited. Content may change prior to final publication. Citation information: DOI 10.1109/TUFFC.2022.3176742, IEEE Transactions on Ultrasonics, Ferroelectrics, and Frequency Control

11

Clutter Filtering for Ultrafast Doppler Imaging Using Similarity of Spatial Singular Vectors," *IEEE Trans. Med. Imaging*, vol. 37, no. 7, pp. 1574–1586, Jul. 2018, doi: 10.1109/TMI.2018.2789499.

[41] J. Zhu *et al.*, "High Frame Rate Contrast-Enhanced Ultrasound Imaging for Slow Lymphatic Flow: Influence of Ultrasound Pressure and Flow Rate on Bubble Disruption and Image Persistence," *Ultrasound Med. Biol.*, vol. 45, no. 9, pp. 2456–2470, 2019, doi: 10.1016/j.ultrasmedbio.2019.05.016.

[42] J. Voorneveld *et al.*, "High-frame-rate contrast-enhanced ultrasound for velocimetry in the human abdominal aorta," *IEEE Trans. Ultrason. Ferroelectr. Freq. Control*, vol. 65, no. 12, pp. 2245–2254, 2018, doi: 10.1109/TUFFC.2018.2846416.

[43] S. A. Waraich, A. Chee, D. Xiao, B. Y. S. Yiu, and A. Yu, "Auto svd clutter filtering for us doppler imaging using 3d clustering algorithm," in *Lecture Notes in Computer Science (including subseries Lecture Notes in Artificial Intelligence and Lecture Notes in Bioinformatics)*, Aug. 2019, vol. 11663 LNCS, pp. 473–483, doi: 10.1007/978-3-030-27272-2_42.

[44] C. M. Gallippi and G. E. Trahey, "Adaptive clutter filtering via blind signal separation for lateral blood velocity measurement," 2002. doi: 10.1109/ULTSYM.2002.1192585.

[45] J. E. Tierney, D. M. Wilkes, and B. C. Byram, "Independent component analysis-based tissue clutter filtering for plane wave perfusion ultrasound imaging," in *Medical Imaging 2019: Ultrasonic Imaging and Tomography*, Mar. 2019, vol. 10955, p. 2, doi: 10.1117/12.2512290.

[46] D. Wang *et al.*, "Numerical and experimental investigation of impacts of nonlinear scattering encapsulated microbubbles on Nakagami distribution," *Med. Phys.*, vol. 46, no. 12, pp. 5467–5477, Dec. 2019, doi: 10.1002/mp.13833.

[47] J. F. Chen, J. A. Zagzebski, and E. L. Madsen, "Non-Gaussian Versus Non-Rayleigh Statistical Properties of Ultrasound Echo Signals," *IEEE Trans. Ultrason. Ferroelectr. Freq. Control*, vol. 41, no. 4, pp. 435–440, 1994, doi: 10.1109/58.294102.

[48] V. Daeichin *et al.*, "Microbubble Composition and Preparation for High-Frequency Contrast-Enhanced Ultrasound Imaging: In Vitro and in Vivo Evaluation," *IEEE Trans. Ultrason. Ferroelectr. Freq. Control*, vol. 64, no. 3, pp. 555–567, Mar. 2017, doi: 10.1109/TUFFC.2016.2640342.

[49] D. Maresca, M. Correia, M. Tanter, B. Ghaleh, and M. Pernot, "Adaptive spatiotemporal filtering for Coronary Ultrafast Doppler Angiography," *IEEE Trans. Ultrason. Ferroelectr. Freq. Control*, vol. 65, no. 11, pp. 2201–2204, 2018, doi: 10.1109/TUFFC.2018.2870083.

[50] B. Arnal, J. Baranger, C. Demene, M. Tanter, and M. Pernot, "In vivo real-time cavitation imaging in moving organs," *Phys. Med. Biol*, vol. 62, pp. 843–857, 2017, doi: 10.1088/1361-6560/aa4fe8.

[51] V. Zarzoso and P. Comon, "Robust independent component analysis by iterative maximization of the kurtosis contrast with algebraic optimal step size," *IEEE Trans. Neural Networks*, vol. 21, no. 2, pp. 248–261, 2010, doi: 10.1109/TNN.2009.2035920.

[52] G. F, V. HJ, M. R, de J. N, and T. P, "Microbubble characterization through acoustically induced deflation," *IEEE Trans. Ultrason. Ferroelectr. Freq. Control*, vol. 57, no. 1, pp. 193–202, Jan. 2010, doi: 10.1109/TUFFC.2010.1398.

[53] P. Song, A. Manduca, J. D. Trzasko, and S. Chen, "Ultrasound Small Vessel Imaging With Block-Wise Adaptive Local Clutter Filtering," *IEEE Trans. Med. Imaging*, vol. 36, no. 1, pp. 251–262, 2017, doi: 10.1109/TMI.2016.2605819.

[54] D. Maresca, M. Correia, M. Tanter, B. Ghaleh, and M. Pernot, "Adaptive spatiotemporal filtering for Coronary Ultrafast Doppler Angiography," *IEEE Trans. Ultrason. Ferroelectr. Freq. Control*, 2018, doi: 10.1109/TUFFC.2018.2870083.

[55] J. J. Kwan and M. A. Borden, "Microbubble dissolution in a multigas environment," *Langmuir*, vol. 26, no. 9, pp. 6542–6548, May 2010, doi: 10.1021/la904088p.

[56] S. Harput *et al.*, "Two-Stage Motion Correction for Super-Resolution Ultrasound Imaging in Human Lower Limb," *IEEE Trans. Ultrason. Ferroelectr. Freq. Control*, vol. 65, no. 5, pp. 803–814, May 2018, doi: 10.1109/TUFFC.2018.2824846.

[57] R. Nayak, V. Kumar, J. Webb, A. Gregory, M. Fatemi, and A. Alizad, "Non-contrast agent based small vessel imaging of human thyroid using motion corrected power Doppler imaging," *Sci. Rep.*, vol. 8, no. 1, 2018, doi: 10.1038/s41598-018-33602-9.

[58] F. Destrempes and G. Cloutier, "A critical review and uniformized representation of statistical distributions modeling the ultrasound echo envelope," *Ultrasound in Medicine and Biology*, vol. 36, no. 7. Elsevier, pp. 1037–1051, Jul. 01, 2010, doi: 10.1016/j.ultrasmedbio.2010.04.001.

[59] D. Wang, D. Liu, Y. Sang, Y. Zhang, M. Wan, and C. J. Diederich, "*In vivo* Nakagami- *m* parametric imaging of microbubble-enhanced ultrasound regulated by RF and VF processing techniques," *Med. Phys.*, vol. 47, no. 11, pp. 5659–5668, Nov. 2020, doi: 10.1002/mp.14474.

Geraldi Wahyulaksana was born in Jakarta, Indonesia in 1992. He got the M.S. degree in electrical engineering from Eindhoven University of Technology, in 2017 after working on contrast agent modelling for MRI. From 2017 to 2019 he worked as a software designer in Son and developed an object detection system for a wireless power transfer system with air-coupled ultrasound. Since 2019 he is currently a Ph.D. student at the Department of Biomedical Engineering, Erasmus Medical Center, Rotterdam, The Netherlands. His current research interest is methods to detect microbubbles with high framerate ultrasound imaging.

This article has been accepted for publication in a future issue of this journal, but has not been fully edited. Content may change prior to final publication. Citation information: DOI 10.1109/TUFFC.2022.3176742, IEEE Transactions on Ultrasonics, Ferroelectrics, and Frequency Control

12

Luxi Wei (M'19) received her B.Sc. degree in honours biophysics from the University of British Columbia, Canada, in 2016 and her M.Sc. degree in medical biophysics from the Univiersity of Toronto, Canada, in 2019. She is currently pursuing a Ph.D. degree at the Department of Biomedical Engineering, Erasmus Medical Center, The Netherlands. Her research includes high frame rate ultrasound, contrast agent imaging, volumetric beamforming techiniques, and transducer development.

Jasper Schoormans was born in Dordrecht, the Netherlands in 1992. He received the M.Sc. degree in applied physics from Technical University Delft, Delft, The Netherlands and the Ph.D. degree in increasing efficiency of MRI acquisition methods from University of Amsterdam in 2020. His current interests are data science and web development.

Jason Voorneveld was born in Johannesburg, South Africa, in 1987. He received the B.Sc. degree in electro-mechanical engineering (2009) and an M.Sc. degree in biomedical engineering (2014) from the University of Cape Town, Cape Town, South Africa. He obtained his Ph.D. degree in biomedical engineering at Erasmus MC, Rotterdam, the Netherlands (2019). He is currently working as a postdoc at Erasmus MC. His research interests include high-frame-rate ultrasound imaging, blood-flow quantification and ultrasound contrast agents.

Antonius F. W. van der Steen (Fellow, IEEE) received the master's degree in applied physics and the Ph.D. degree in medical sciences. He is currently the Head of Biomedical Engineering at the Thorax Centre, Erasmus MC. He is an expert in ultrasound, cardiovascular imaging, and cardiovascular biomechanics. He has a career at the crossroads of Engineering, Health Care, and Industry. He has experience in running large consortia as the Co-Founder and former Chairman of the Medical Delta, which comprises of over 280 scientists working on technical solutions for sustainable health. He was also the Co-PI of ParisK, one of the large CTMM projects (16 MEuro). His international profile is high, with more than 200 invited lectures all over the world, and Guest Professorship/Guest Researcher in Canada, Japan, and China. Dr. van der Steen is a fellow of the European Society of Cardiology. He is a member of the Netherlands Academy of Technology (AcTI) and a board member of the Royal Netherlands Academy of Sciences (KNAW). He is a recipient of the Simon Stevin Master Award, and the NWO PIONIER Award in Technical Sciences.

Nico de Jong graduated from the Delft University of Technology, The Netherlands, in 1978. He received the M.Sc. degree in applied physics in the field of pattern recognition, and the Ph.D. degree in acoustic properties of ultrasound contrast agents, in 1993. From 2003 to 2011, he was a part-time Professor with the University of Twente in the group Physics of Fluids headed by Prof. Detlef Lohse. He is currently the Vice Head of Biomedical Engineering with the Thoraxcenter, Erasmus University Medical Center, Rotterdam, headed by Prof. Ton van der Steen. He is the Head of the Medical Imaging Group, Technical University, Delft. He is the Founder and an Organizer of the Annual European Symposium (this year for the 25th time, see http://www.echocontrast.nl) on ultrasound contrast imaging, held in Rotterdam and attended by approximately 175 scientists from universities and industries all over the world. He is on the safety committee of the World Federation of Ultrasound in Medicine and Biology (WFUMB). He is an Associate Editor of Ultrasound in Medicine and Biology and the IEEE Transactions on Ultrasonics, Ferroelectrics, and Frequency Control. He has been a guest editor for special issues of several journals. He teaches on Technical Universities and the Erasmus MC. He has graduated 38 Ph.D. students and is currently supervising more than 12 Ph.D. students.

Hendrik J. Vos (M '14) received the M.Sc. degree in Applied Physics from Delft University of Technology, Delft, The Netherlands in 2004, and his Ph.D. degree with the Department of Biomedical Engineering at Erasmus MC, Rotterdam, The Netherlands, in 2010. He worked as a Postmaster Researcher with the University of Florence, Italy, and as a contract researcher for the petrochemical industry on cutting-edge ultrasonic solutions. He currently is associate professor with Erasmus MC and Delft University of Technology, and received a Dutch NWO-TTW-VIDI personal grant in 2018. His research interests include acoustical array technology for biomedical imaging in all its aspects: transducers, 2-D and 3-D beamforming, cardiac shear waves, ultrafast Doppler, contrast imaging, and related subclinical and clinical studies.